

# Dark matter response to galaxy formation

Patricia B. Tissera<sup>1,2\*</sup>, Simon D. M. White<sup>3</sup>, Susana Pedrosa<sup>1,2</sup> and Cecilia Scannapieco<sup>4</sup>

<sup>1</sup> *Consejo Nacional de Investigaciones Científicas y Técnicas, CONICET, Argentina.*

<sup>2</sup> *Instituto de Astronomía y Física del Espacio, Casilla de Correos 67, Suc. 28, 1428, Buenos Aires, Argentina. CONICET-UBA*

<sup>3</sup> *Max-Planck Institute for Astrophysics, Karl-Schwarzschild Str. 1, D85748, Garching, Germany*

<sup>4</sup> *Astrophysikalisches Institut Potsdam, An der Sternwarte 16, D-14482 Potsdam, Germany*

22 October 2018

## ABSTRACT

We have resimulated the six galaxy-sized haloes of the Aquarius Project including metal-dependent cooling, star formation and supernova feedback. This allows us to study not only how dark matter haloes respond to galaxy formation, but also how this response is affected by details of halo assembly history. In agreement with previous work, we find baryon condensation to lead to increased dark matter concentration. Dark matter density profiles differ substantially in shape from halo to halo when baryons are included, but in all cases the velocity dispersion decreases monotonically with radius. Some haloes show an approximately constant dark matter velocity anisotropy with  $\beta \approx 0.1 - 0.2$ , while others retain the anisotropy structure of their baryon-free versions. Most of our haloes become approximately oblate in their inner regions, although a few retain the shape of their dissipationless counterparts. Pseudo-phase-space densities are described by a power law in radius of altered slope when baryons are included. The shape and concentration of the dark matter density profiles are not well reproduced by published adiabatic contraction models. The significant spread we find in the density and kinematic structure of our haloes appears related to differences in their formation histories. Such differences already affect the final structure in baryon-free simulations, but they are reinforced by the inclusion of baryons, and new features are produced. The details of galaxy formation need to be better understood before the inner dark matter structure of galaxies can be used to constrain cosmological models or the nature of dark matter.

**Key words:** galaxies: haloes, galaxies: structure, cosmology: dark matter

## 1 INTRODUCTION

Dissipationless cosmological simulations have contributed substantially to our understanding of the structure and evolution of cold dark matter (CDM) haloes, showing them to have triaxial shapes (Frenk et al. 1998; Dubinski & Carlberg 1991; Jing & Suto 2002; Hayashi, Navarro & Springel 2007) and density profiles with inner cusps (Dubinski & Carlberg 1991, Navarro, Frenk & White 1996; Moore et al. 1999; Diemand et al. 2005) and an approximately universal shape, independent of mass or cosmological parameters (Navarro, Frenk & White 1997). This universal cuspy profile appears in conflict with several observations, for example, the slow increase of rotation velocity with radius at the centre of low surface brightness galaxies (Flores & Primack 1994; McGaugh & de Blok 1998; Moore et al 1999; Salucci, Yegorova & Drory 2008) and the relatively weak concentration of galaxy clusters inferred from strong lensing (Sand et

al. 2008). Additional evidence supporting central dark matter densities lower than predicted by CDM models comes from the difficulty in simultaneously matching observed luminosity functions and the zero-point of the Tully-Fisher relation (e.g. Dutton, van den Bosch & Courteau 2008). Recently, Navarro et al. (2008, hereafter N08) analysed in detail the density profiles of very high-resolution dark matter-only simulations of six Milky Way mass haloes from the Aquarius Project (Springel et al. 2008). They found the innermost cusps in these haloes to be weaker than claimed in some earlier work, and showed how halo-to-halo variations in radial structure reflect the detailed formation histories of individual haloes (see also Vogelsberger et al. 2009).

Galaxy formation might reinforce such history-specific features in the dark matter distribution, since baryons are subject to dissipative processes such as cooling, star formation and feedback in addition to gravity. The condensation of baryons within dark matter haloes modifies both their dynamics and their structure, but exactly how this happens is still quite uncertain. The simplest model assumes that

\* E-mail: patricia@iafe.uba.ar

the dark halo is compressed radially and adiabatically by the added mass at its centre (Blumenthal et al. 1986, hereafter B86; see Eggen et al. 1962, Zeldovich et al. 1980 and Barnes & White 1984 for previous applications of this formalism). Recent simulations have found the very simple adiabatic compression (AC) scheme of B86 to overestimate the effect (e.g. Gnedin et al. 2004 and Abadi et al. 2009, hereafter G04 and A09, respectively; Pedrosa, Tissera & Scannapieco 2010) but it is nevertheless often used in simplified modelling of galaxy formation (e.g. Mo, Mao & White 1998). More sophisticated AC models, based, for example, on the formalism of Young (1980) have claimed to reproduce better the contraction and the final shape of haloes (G04; Sellwood & McGaugh 2005). The common outcome of these schemes is nevertheless an increase in the dark matter density in the central regions, exacerbating the problem of reconciling  $\Lambda$ CDM models with observation.

Simulations of galaxy formation which follow both dark matter and baryons in their proper cosmological context are the primary tool for studying how galaxy assembly affects dark matter haloes. There are many papers devoted to this subject. Improving numerical algorithms and increasing computer power have led to continual progress in understanding the complex interplay between these two components. Previous analyses of the evolution of dark haloes in hydrodynamical simulations have reported an increase both of the central mass concentration and of the central velocity dispersion, which no longer shows the 'temperature inversion' characteristic of dissipationless CDM haloes (e.g. Katz & Gunn 1991; Evrard, Summers & Davis 1994; Navarro & White 1994; Tissera & Domínguez-Tenreiro 1998; Oñorbe et al. 2008; Romano-Díaz et al. 2008). Recently, Pedrosa, Tissera & Scannapieco (2009, 2010) investigated how baryonic assembly history affects the dark matter distribution. They found the SN feedback process to play a key role by regulating star formation activity and ejecting material not only from the main system, but also from infalling satellites. It seems clear that the final distribution of baryons at the centre of a halo is insufficient to determine halo response to galaxy assembly, thus contradicting the AC hypothesis.

Typical dark matter haloes have long been reported to be triaxial with major to minor axis ratios often exceeding two in CDM-only simulations (e.g. Barnes & Efstathiou 1987; Frenk et al. 1988; Dubinski & Carlberg 1991; Jing & Suto 2002; Hayashi, Navarro & Springel 2007). However, their shape changes, becoming more nearly oblate as baryons condense within them (Katz & Gunn 1991; Evrard et al. 1994; Tissera & Domínguez-Tenreiro 1998; Kazantzidis et al. 2004; Debattista et al. 2008; A09). These results suggest the need for a comprehensive analysis of halo structure in simulations which include both the appropriate cosmological context and a realistic description of the physics of baryon condensation. It is clearly necessary to analyse a number of different galaxy-sized haloes in order to explore how differing assembly histories affect the structure of the final haloes.

In this paper, we study a set of high-resolution resimulations of the six galaxy-mass haloes of the Aquarius Project (Springel et al. 2008). These were carried out with a version of GADGET-3 which includes a multi-phase treatment of metal-dependent cooling, star formation and SN feedback (Scannapieco et al. 2005, 2006). The original haloes were selected from a cosmological CDM-only simulation with no re-

striction on merger history, except that implied by eliminating objects with high-mass close neighbours. This Aquarius halo set is well-suited to study how formation history and baryonic condensation together determine the final structure of dark matter haloes. Our ability to isolate these effects is aided by comparing results from our hydrodynamical simulations (hereafter SPH runs) with corresponding results from the CDM-only simulations (hereafter DM runs) as reported by N08. Properties of the galaxies in these haloes are studied in Scannapieco et al. (2009) and will be further analysed in a forthcoming paper.

This paper is organized as follows. In Section 2, we describe the numerical experiments. In Section 3, we analyse the dark matter density profiles. Section 4, describes the velocity dispersion structure of our haloes. In Section 5, we study the effects of baryons on the pseudo-phase-space density profile, while Section 6 discusses halo shapes. Section 7 compares the change in halo circular velocity profile between the SPH and the DM runs with the predictions of AC models. Finally, in Section 8, we summarize our main findings.

## 2 THE SIMULATED HALOES

The six haloes studied in this paper were taken from the Aquarius Project (Springel et al. 2008). They were selected at random from a lower resolution version of the  $(100 h^{-1}\text{Mpc})^3$  Millennium-II Simulation (Boylan-Kolchin et al. 2009) subject only to the requirements that their mass should be similar to that inferred for the Milky Way's halo and that they should have no close massive neighbour. Dark matter only versions of these haloes were then resimulated at a variety of much higher resolutions as part of the Aquarius Project itself (Springel et al. 2008; N08; Vogelsberger et al. 2009). The lowest resolution version of each halo (designated as resolution level 5) was also resimulated with detailed modelling of baryonic processes by Scannapieco et al. (2009, hereafter S09). Details of how the initial conditions were created can be found in these two papers. In the following we will refer to the original Aquarius simulations at the higher resolution level 2 as the DM simulations, and to the simulations of S09, which have roughly 200 times worse dark matter mass resolution but include the baryonic physics, as the SPH simulations. The analysis in N08 shows that the properties of the dark haloes which concern us in this paper are extremely well numerically converged all the way down to resolution level 5. The individual haloes are labelled Aq-A- $n$ , Aq-B- $n$ , etc., with  $n$  corresponding to the resolution level in to be consistent with the convention in the earlier papers.

The Millennium and Millennium-II Simulations, and thus also these halo simulations, were carried out assuming a  $\Lambda$ CDM cosmology with parameters  $\Omega_m = 0.25$ ,  $\Omega_\Lambda = 0.75$ ,  $\sigma_8 = 0.9$ ,  $n_s = 1$  and  $H_0 = 100 h \text{ kms}^{-1}\text{Mpc}^{-1}$  with  $h = 0.73$ . Evolution in both the DM and the SPH simulations was followed from  $z = 127$  to  $z = 0$  using versions of GADGET-3, an update of GADGET-2 (Springel et al. 2001; Springel 2005) optimized for massively parallel simulation of highly inhomogeneous systems such as individual dark haloes.

The version of GADGET-3 used for the SPH runs

includes a multiphase model for the gas component with metal-dependent cooling, star formation and phase-dependent treatments of SN feedback and chemical enrichment, as set out in Scannapieco et al. (2005, 2006) and employed for studying  $\Lambda$ CDM galaxy formation in Scannapieco et al. (2008, 2009). The model describes chemical enrichment by SNII and SNIa separately, using appropriate yields and delays (Mosconi et al. 2001; Scannapieco et al. 2005). The multiphase treatment of both hydrodynamics and feedback is quite effective in reproducing the observed phenomenology of star formation and wind-generation in both quiescent and starburst galaxies. Without introducing system-specific parameters, the scheme produces substantial mass-loaded galactic winds in rapidly star-forming systems with speeds that reflect the escape velocity much as in observed galaxies (Scannapieco et al. 2006, 2008). This freedom from *ad hoc* scale-dependent parameters, makes the algorithm particularly suited for studying galaxy formation in its cosmological context, since the simultaneous formation of systems of widely differing mass is the norm in this situation.

The SPH runs have maximum gravitational softenings in the range  $\epsilon_G = 0.5 - 1 h^{-1}\text{kpc}$ . To prevent spurious results due to limited numerical resolution in the innermost regions, we analyse halo properties only outside  $2h^{-1}\text{kpc}$  in all our systems. Haloes are considered bounded by their virial radius  $r_{200}$  defined as the largest radius within which the mean enclosed density exceeds  $\approx 200$  times the critical density. The simulated SPH haloes have  $\approx 1$  million particles in total within this virial radius while the DM simulations have approximately  $10^8$  particles in the same region. The virial masses of the six systems are in the range 5 to  $11 \times 10^{11} h^{-1} M_\odot$ . Hence, dark matter particles in the SPH runs have masses of the order  $10^6 h^{-1} M_\odot$  while gas particles initially have  $\approx 2 \times 10^5 h^{-1} M_\odot$ . In Table 1 we summarize the principal characteristics of our SPH simulations. We also include the corresponding information for two lower resolution versions of halo Aq-E. We find convergent results between Aq-E-5 and Aq-E-6 for their characteristic properties. However, for the lowest resolution run, Aq-E-7, larger differences are found. In Section 3, we discuss the effects of numerical resolution on the dark matter distributions.

The Aquarius haloes have varied assembly histories and these produce a variety of structures and star formation histories for their central galaxies, even though the simulations were all run with similar SF and SN feedback parameters. A detailed description of the code and the parameters adopted can be found in S09, together with images of the central galaxies and considerable analysis of their structure. Here we provide a brief summary so that the reader has a general picture of the central galaxies of the haloes we analyse here.

In all six galaxies star formation peaked between 13 Gyr (Aq-C-5) and 10 Gyr (Aq-B-5) ago and there has been rather little star formation over the last 8 Gyr. The total stellar masses at  $z = 0$  are in the range  $2.5$  to  $6 \times 10^{10} h^{-1} M_\odot$  and are listed in Table 1, along with the total masses and baryon masses of the  $z = 0$  haloes and the numbers of simulation particles representing these masses.

The analysis of S09 showed that most of the central galaxies contain centrifugally supported disks, although none of these accounts for more than about a fifth of the total stellar mass. Aq-F-5 is an exception in that it has no disk, only a spheroidal component. This can be traced to the

fact that the system underwent a major merger at  $z \sim 0.6$ . In some cases the stellar spheroid has substantial net rotation (Aq-E-5) while in others it retains very little angular momentum (Aq-A-5). All the galaxies have been substantially affected by SN feedback, which drives winds which limit their mass. In all cases the baryon fraction within the virial radius is around 10%, significantly smaller than the global value,  $f_b = 0.16$ .

### 3 DARK MATTER DENSITY PROFILES

We have constructed spherically-averaged dark matter density profiles from  $2 h^{-1}\text{kpc}$  to the virial radius  $r_{200}$ . The inner radius is four times the gravitational softening for three of our simulations (A, B and D) and twice the gravitational softening in the other three. It typically contains more than a thousand dark matter particles. Finding an appropriate centre is crucial to obtaining accurate profiles. Here we use the shrinking sphere technique as laid out in Power et al. (2003). In practise, this gives a centre very close to the minimum of the gravitational potential in all our systems. We have measured profiles both including and excluding substructures, but this only causes rather minor effects in the outer regions. In the following we use the full DM mass including substructures in order to be able to compare consistently with the results of N08. Note that we re-normalize the dark matter profiles of N08 by the global DM fraction of 0.84 adopted in the SPH simulations when comparing profiles from the two set-ups.

To characterise our dark matter profiles we adopt the three-parameter Einasto model (Einasto 1965) which N08 found to give a relatively good fit to the profiles of the DM runs. This model has also been used by earlier authors to fit the dark matter distribution when baryons are included (e.g. Oñorbe et al. 2008; Gao et al. 2008). N08 parametrise the Einasto profile using  $\alpha$ ,  $r_{-2}$  and  $\rho_{-2}$ , which indicate its curvature in a log-log plot, and the radius and density at the point where its logarithmic slope is  $-2$ , the isothermal value. We fit this formula, leaving all three parameters free, to our measured density profile at a set of points spaced logarithmically from  $2 h^{-1}\text{kpc}$  to  $r_{200}$ , minimising the rms residual in  $\log \rho$ . In Table 2 we give the results of these fits, together with the rms residual in  $\log \rho$ . To facilitate the comparison with the DM runs, we also include the corresponding parameters given by N08; note that these were obtained for fits over a slightly wider radial range. We see that in all cases  $r_{-2}$  and  $\alpha$  are both smaller for the simulations which include baryons, showing that the condensation of the galaxy has increased the concentration of the halo and given it a density profile which is approximately isothermal over a wider radial range than in the DM-only case. The residuals in  $\log \rho$  are only slightly larger, showing that the Einasto profile is a good fit to both the SPH and the DM runs.

This is evident in Fig. 1 where we compare the spherically-averaged dark matter density profiles of the haloes in our SPH runs (solid lines) to the corresponding profiles for the DM runs from N08 (dashed lines). Every SPH profile lies below its corresponding DM profile at large radii and above it at small radii. In all cases the two profiles cross at, or slightly inside, the baryonic radius of the central galaxy, which we define to be the radius containing 83% of

**Table 1.** General characteristics of our Aquarius halo simulations and their central galaxies. The first column show the halo name, taken from Springel et al. (2008).  $\epsilon_G$  is the gravitational softening.  $r_{200}$  and  $M_{200}$  are the radius and mass of the sphere enclosing total mean mass density 200 times the critical value.  $M_{\text{dm}}$  and  $M_{\text{bar}}$  are dark matter and baryonic masses within this same sphere.  $M_s$  is the stellar mass of the main galaxy hosted by each halo, measured within an optical radius defined to contain 83% of the galaxy’s baryonic mass.  $N_{\text{dm}}$  and  $N_{\text{bar}}$  are the total number of particle representing each mass component.

Halo	$\epsilon_G$ kpc h <sup>-1</sup>	$r_{200}$ kpc h <sup>-1</sup>	$M_{200}$ 10 <sup>12</sup> M <sub>⊙</sub> h <sup>-1</sup>	$M_{\text{dm}}$ 10 <sup>11</sup> M <sub>⊙</sub> h <sup>-1</sup>	$M_{\text{bar}}$ 10 <sup>10</sup> M <sub>⊙</sub> h <sup>-1</sup>	$M_s$ 10 <sup>10</sup> M <sub>⊙</sub> h <sup>-1</sup>	$N_{\text{dm}}$	$N_{\text{bar}}$
Aq-A-5	0.5	169.42	1.10	9.95	10.17	5.92	529110	425737
Aq-B-5	0.5	132.10	0.52	4.79	4.15	2.53	435330	354976
Aq-C-5	1.0	173.19	1.18	10.70	10.68	5.93	681143	647325
Aq-D-5	0.5	170.63	1.09	10.10	8.29	4.41	599438	460845
Aq-E-5	1.0	149.93	0.79	7.08	8.05	4.97	554245	606136
Aq-F-5	1.0	142.74	0.67	5.99	6.92	5.39	680129	759456
Aq-E-6	2.0	150.79	0.79	7.20	7.60	4.89	132662	132698
Aq-E-7	4.0	146.39	0.73	6.75	5.41	3.06	44429	32214

**Table 2.** Characteristics of the density profiles of the haloes in our Aquarius galaxy formation simulations. Column (1) gives the name of each halo. Columns (2),(3) and (4) list  $\alpha$ ,  $r_{-2}$  and  $\rho_{-2}$  (in units of kpc h<sup>-1</sup> and M<sub>⊙</sub>h<sup>2</sup>kpc<sup>-3</sup>), the parameters of the best fitting Einasto model. Column (5) gives the *rms* scatter in log  $\rho$  around this fit. Column (6) lists exponents for the best power law fits to  $\rho/\sigma^3$  as a function of  $r$ . Columns (7), (8) (9) (10) and (11) list the corresponding fitting parameters for the corresponding DM runs. Note that the fitting parameters for the profiles in the DM runs differ slightly from those given by N08 because we have re-calculated them over the same radial range used for the SPH runs.

Run	$\alpha$	$r_{-2}$	log $\rho_{-2}$	<i>rms</i>	$\chi$	$\alpha^{\text{DM}}$	$r_{-2}^{\text{DM}}$	log $\rho_{-2}^{\text{DM}}$	<i>rms</i>	$\chi^{\text{DM}}$
Aq-A-5	0.065	3.68	7.81	0.016	-1.67	0.108	13.13	6.71	0.001	-2.05
Aq-B-5	0.145	10.95	6.59	0.015	-1.63	0.192	16.64	6.28	0.007	-1.87
Aq-C-5	0.115	7.17	7.28	0.014	-1.63	0.179	13.58	6.76	0.010	-1.95
Aq-D-5	0.102	10.35	6.85	0.018	-1.66	0.178	21.23	6.28	0.008	-1.86
Aq-E-5	0.098	7.79	6.99	0.017	-1.62	0.149	14.97	6.47	0.010	-1.91
Aq-F-5	0.112	10.89	6.62	0.011	-1.60	0.164	18.96	6.22	0.016	-1.98
Aq-E-6	0.091	7.77	6.99	0.012	-1.68	–	–	–	–	–
Aq-E-7	0.15	14.69	6.41	0.013	-1.96	–	–	–	–	–

its stars and cold gas. Inside the baryonic radius, the SPH profiles are all relatively flat, and so approximately “isothermal”. This is indicated more explicitly in the insets in Fig. 1 which plot the logarithmic derivatives of the two profiles as a function of radius. This slope changes smoothly with radius in most of the DM haloes, but shows a clear change in behaviour in the inner regions in many of the SPH haloes. For Aq-A-5, Aq-C-5 and Aq-E-5, we detect a change in the logarithmic derivatives of the SPH profiles at the smallest radii suggesting a flattening of the profiles. However, this occurs very close to our resolution limit and therefore, should be viewed with caution. At radii well outside the central galaxy the SPH profiles parallel the DM profiles quite closely, and indeed the offset between them is close to the renormalisation factor that we introduced to account for the difference in the total amount of dark matter in the two kinds of simulation.

We have looked for correlations between the changes in  $\alpha$  and  $r_{-2}$  and various other parameters of our haloes, in particular, their spin parameter, the fraction of the baryons gathered in the central galaxy, and their disk-to-total mass ratio. However, in no case did we find a clear trend.

To study the robustness of our results against numerical resolution, we analysed the dark matter profiles of the two lower resolution versions of halo Aq-E. The results show ex-

cellent convergence for the dark matter profile and its characteristic properties, as can be seen in Fig. 1. Runs Aq-E-5 and Aq-E-6 are in very good agreement over the whole analysed region. The same is true for the lowest resolution Aq-E-7 but only over the region resolved with at least a thousand dark matter particles. A lower resolution seems to produce an underestimation of the dark matter density in the innermost regions. In Table 2, we include the fitting parameters for these two additional simulations (carried out from twice their gravitational softening). Based on these findings, we are confident that our main set of simulations have been run with adequate numerical resolution to assure convergent results for the density profiles over the analysed radial interval.

#### 4 VELOCITY DISPERSION DISTRIBUTIONS

The velocity dispersion structure of the dark matter haloes in the DM runs has been analysed by N08, who show that they all have a temperature inversion in the central region (i.e. the velocity dispersion drops towards the centre at small radii) but that there is no simple regularity among the haloes. Rather there is considerable diversity which seems

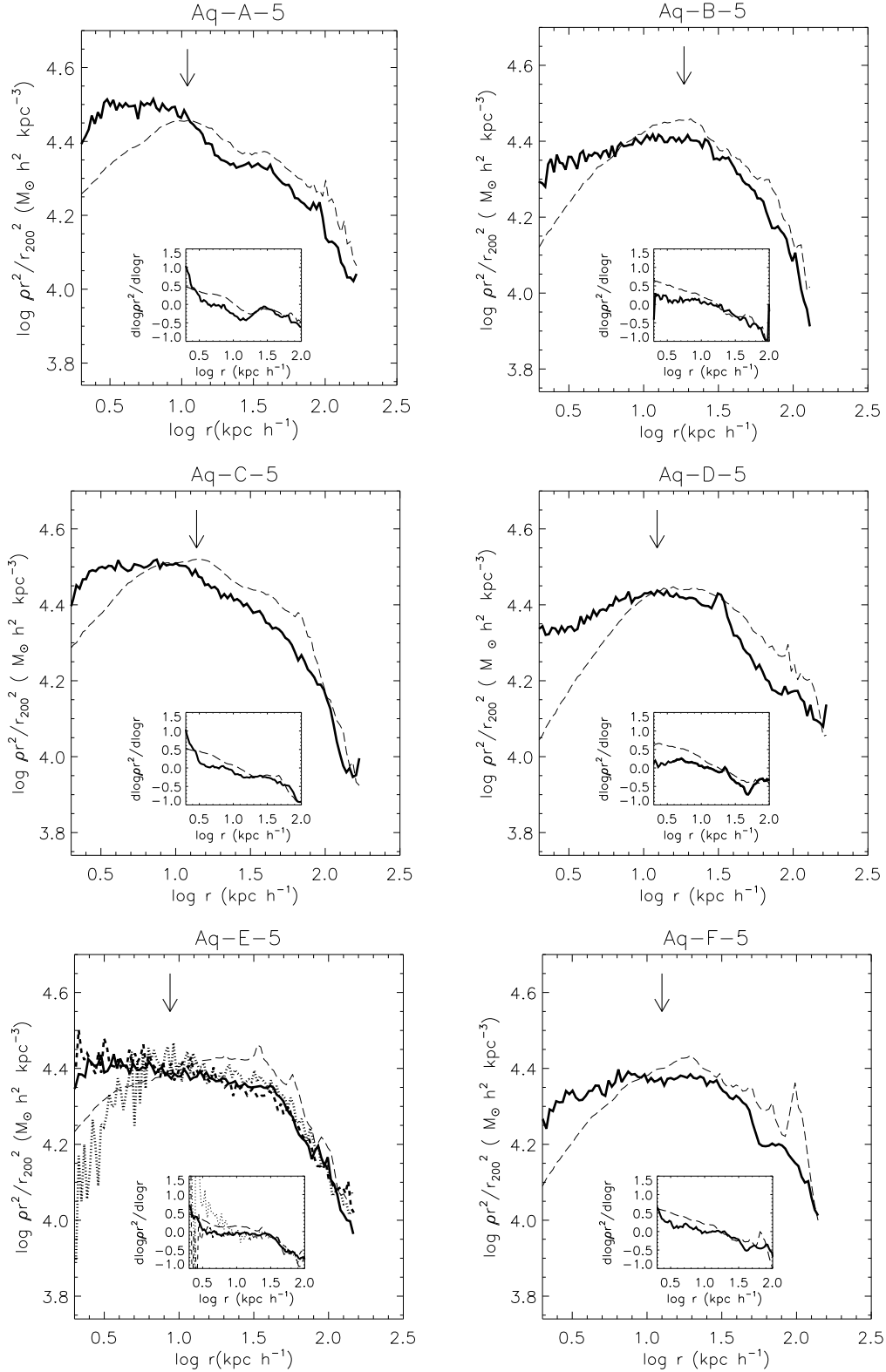


**Figure 1.** Spherically-averaged dark matter profiles for six haloes from the Aquarius Project simulated with (solid lines) and without (long dashed lines) baryons. We plot the profiles from  $2 h^{-1} \text{kpc}$  to the virial radius  $r_{200}$ . The DM runs are the resolution level 2 simulations studied by Navarro et al. (2008). The arrow indicates the baryonic radius of the central galaxy defined as the radius enclosing 83% of its stars and cold gas. The inset boxes show the logarithmic derivatives of the profiles. We include the lower resolution versions of Aq-E: Aq-E-6 (short-dashed lines) and Aq-E-7 (dotted lines).

to reflect the variety of formation paths possible for these galaxy-sized haloes in the  $\Lambda$ -CDM cosmology.

We here carry out a similar analysis of the velocity dispersion structure of our set of SPH runs. In Fig. 2 we compare their total velocity dispersion profiles to those of the DM runs. It is clear that the baryons have substantially affected the velocities of dark matter particles within the baryonic radius of the central galaxy. As reported in previous work (e.g. Tissera & Dominguez-Tenreiro 1998; Romano-Diaz et al. 2008; Pedrosa et al. 2010) the increased velocity dispersion in the central regions results in a final profile that decreases monotonically with radius, in contrast to the behaviour seen in DM-only simulations. For Aq-E-5, we have included its lower resolution versions (Aq-E-6 and Aq-E-7). As can be seen, the lowest resolution version provides a poor representation of the velocity distribution obtained with the higher resolution runs. However, Aq-E-6 and Aq-E-5 agree very well except in the very central region.

The conventional velocity anisotropy parameter, defined as  $\beta(r) \equiv 1 - \sigma_t^2/(2\sigma_r^2)$  where  $\sigma_t$  and  $\sigma_r$  are tangential and radial dispersions averaged over spherical shells, gives some indication of the internal orbital structure of the haloes. As shown by N08, the DM runs are almost isotropic ( $\beta \approx 0$ ) in their inner regions, then in most cases become progressively more radially biased ( $\beta > 0$ ) with increasing radius out to about  $r_{-2}$  before becoming more isotropic again at even larger radii. There are however, substantial differences between the individual haloes. We find that baryonic effects modify the dispersion structure within these haloes in a complicated way, as can be seen in Fig. 3. While some of the SPH haloes have similar anisotropy structure to their DM counterparts (Aq-A-5, Aq-C-5 and Aq-D-5), others have become less dominated by radial motions (Aq-F-5, Aq-B-5 and Aq-E-5). All our haloes remain slightly radially biased,  $\beta \approx 0.1 - 0.2$ , in the inner resolved regions. The lower resolution versions of Eq-E (Aq-E-6 and Aq-E-7) show a large level of noise around the trend determined by the highest resolution run (Aq-E-5). In order to get further insight into the effects of baryons, we plot  $\sigma_t^2$  against  $\sigma_r^2$  in Fig. 4 both for the SPH runs and for their DM counterparts. For the DM runs, nearly isotropic behaviour is evident in the cool central regions ( $r < r_{-2}$ ; magenta circles, radius increasing with dispersion) with an inversion of the relation in the outer regions where radial motions dominate (blue circles radius increasing with decreasing dispersion). Baryon condensation (either by infall or mergers) increases both radial and tangential dispersions and changes the shapes of orbits in the central regions. (Note that the axis ranges of the main plots and of their insets are different). However, each halo has its own particular distribution. Haloes Aq-B-5, Aq-E-5 and Aq-F-5, which have approximately constant velocity anisotropy, are also those that have an almost isothermal density profile to radii larger than the baryonic radius of their central galaxy, as is evident from the insets of Fig. 1.

Finally, we look at the relation between the logarithmic slope of the density profile ( $\gamma(r)$ ) and the velocity anisotropy parameter ( $\beta(r)$ ). Hansen & Moore (2006) suggested that there might be a “universal” relation between these parameters in dissipationless haloes. N08 found that their DM haloes follow a well-defined relation only in the central regions where both parameters are monotonic functions

of  $r$ . In Fig. 5 we show the anisotropy-slope relation for our SPH runs. As can be seen, there are two different behaviours. Three of the haloes (Aq-A-5, Aq-C-5 and Aq-F-5) show similar and well-defined relations over the rough range  $2 h^{-1}\text{kpc} < r < r_{-2}$ , which are fairly close to the HM06 relation. However, for  $r > r_{-2}$ , each halo behaves differently. In general, they show large variations in  $\beta$  (which differ from halo to halo) but relatively minor variations in  $\gamma$  (compare with Fig. 1). For the other haloes (Aq-B-5, Aq-D-5 and Aq-E-5) the logarithmic slope shows only a weak dependence on radius in the region dominated by baryons, consistent with a nearly isothermal profile, while the anisotropy varies from  $\sim 0.1$  to  $\sim 0.4$ . As a result the HM06 relation fails dramatically in these cases.

## 5 THE PHASE-SPACE DENSITY PROFILE

Taylor & Navarro (2001) noticed that the quantity  $Q(r) = \rho(r)/\sigma(r)^3$  is well approximated by a power law  $Q(r) \propto r^{-\alpha}$  with  $\alpha \approx 1.875$  over more than 2.5 orders of magnitude in radius in simulated dark matter haloes of any mass in a CDM cosmology (see also, Rasia, Tormen & Moscardini 2004; Ascsibar et al. 2004; Vass et al. 2008, N08). This is the behaviour predicted in the spherical similarity solution of Bertschinger (1985). This  $Q(r)$  is related to the entropy distribution within haloes, but the origin of its power law behaviour and its relation to structure formation are not yet understood. The apparent universality is established only for pure dark matter haloes and may be broken by the effects of baryons which modify both the velocity dispersion and the density profiles of the dark matter.

As may be seen in Fig. 6, where we show  $Q(r)$  for both the SPH and the DM runs, all our SPH haloes show a less steep relation than their DM counterparts or predicted by Bertschinger’s (1985) similarity solution. The residuals (small boxes in Fig. 6) show that the modified profile is still well fit by a power law at most radii although in a couple of cases (in particular Aq-A-5) there is some indication for deviations in the innermost region. In Table 2 we give the best fit power-law indices for the SPH haloes over the radial range  $2 h^{-1}\text{kpc} < r < r_{200}$ . Interestingly, but not surprisingly considering our previous findings, the level of departure from the Bertschinger value depends on the halo.

It could be possible that the contraction of the dark matter proceeds adiabatically and that the detected increase in entropy at each radius merely reflects the contraction itself. To investigate this point, we plot  $Q$  as a function of enclosed dark matter mass (relative to the total dark matter mass within  $r_{200}$ ) rather than as a function of  $r$ . If the contraction were purely adiabatic, the SPH haloes should show identical behaviour to their DM counterparts when  $Q(r)$  is plotted against  $M(r)/M_{200}$  in this way. As shown in Fig. 7, this is not the case in any of our haloes.

The lower numerical resolution versions of Aq-E do not show significant differences in the pseudo-phase-space density profiles with respect to Aq-E-5 as can be seen from Fig. 6, because the numerical effects in the density and velocity profiles compensate each other. However, if this relation is plotted as a function of the enclosed mass as seen in Fig. 7 the differences are slightly larger.

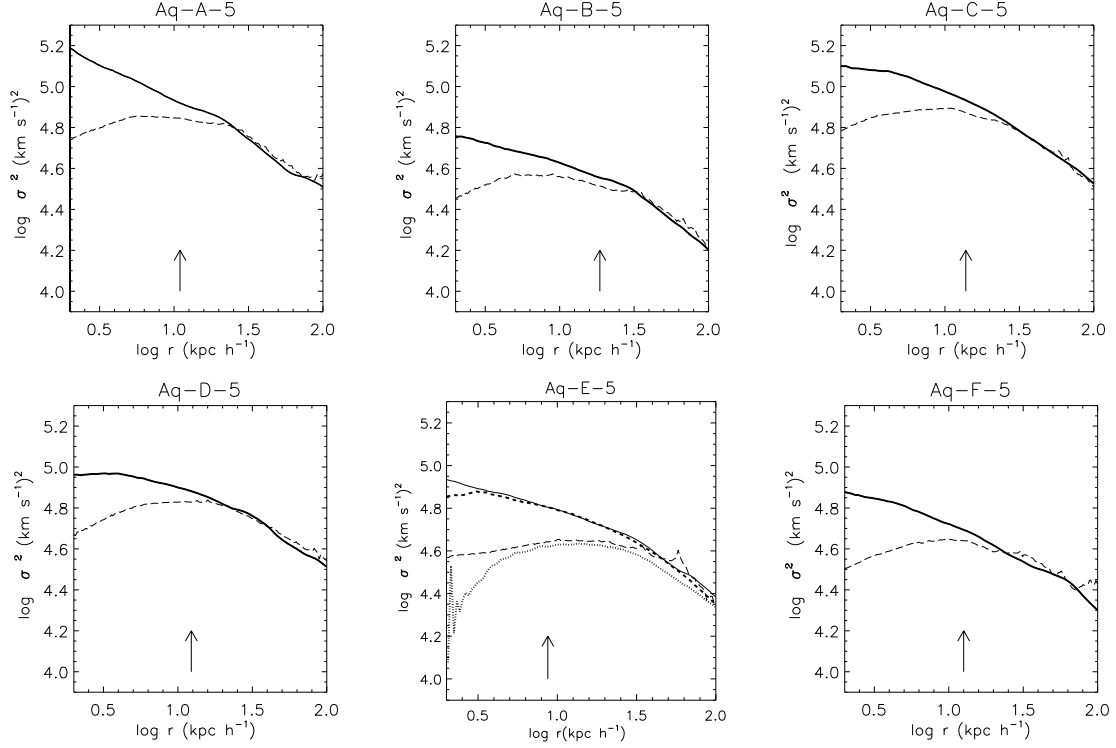


**Figure 2.** Velocity dispersion as a function of radius for the SPH (solid lines) and DM (dashed lines) haloes. The arrows indicate the baryonic radii of the central galaxies. We include the lower resolution versions of Aq-E: Aq-E-6 (short dashed lines) and Aq-E-7 (dotted lines).

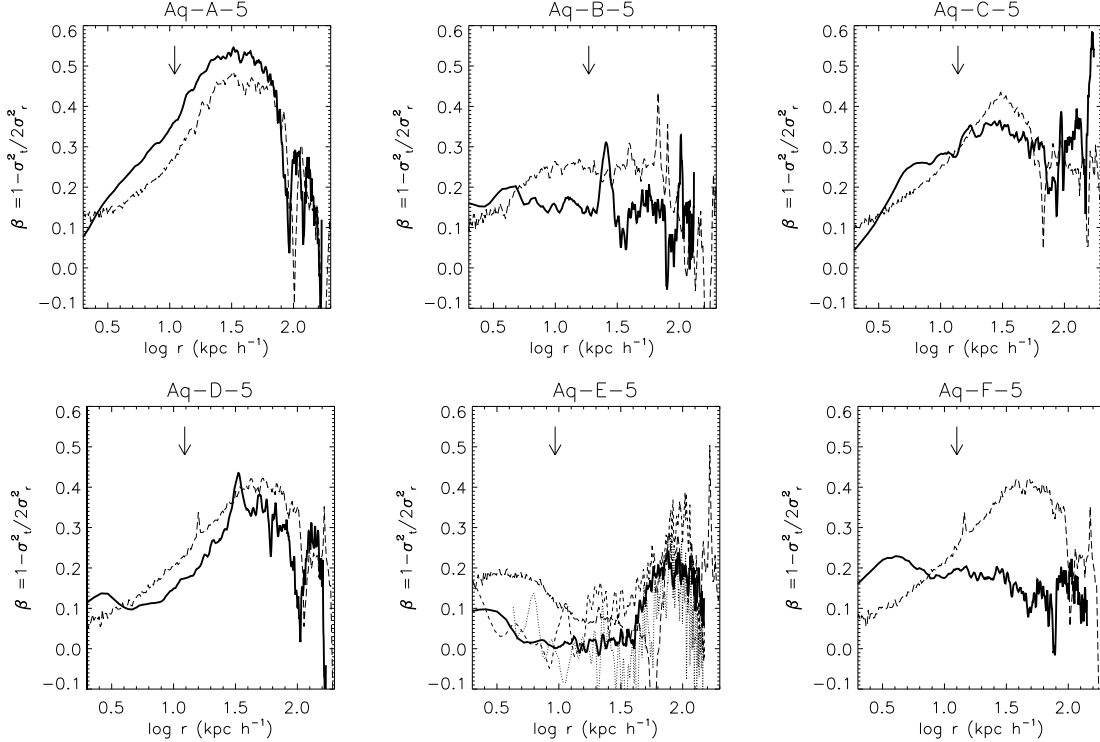


**Figure 3.** Anisotropy parameter ( $\beta$ ) as a function of radius for the SPH (solid lines) and DM (dashed lines) runs. The arrows indicate the baryonic radii of the central galaxies. We include the lower resolution versions of Aq-E: Aq-E-6 (short dashed lines) and Aq-E-7 (dotted lines).

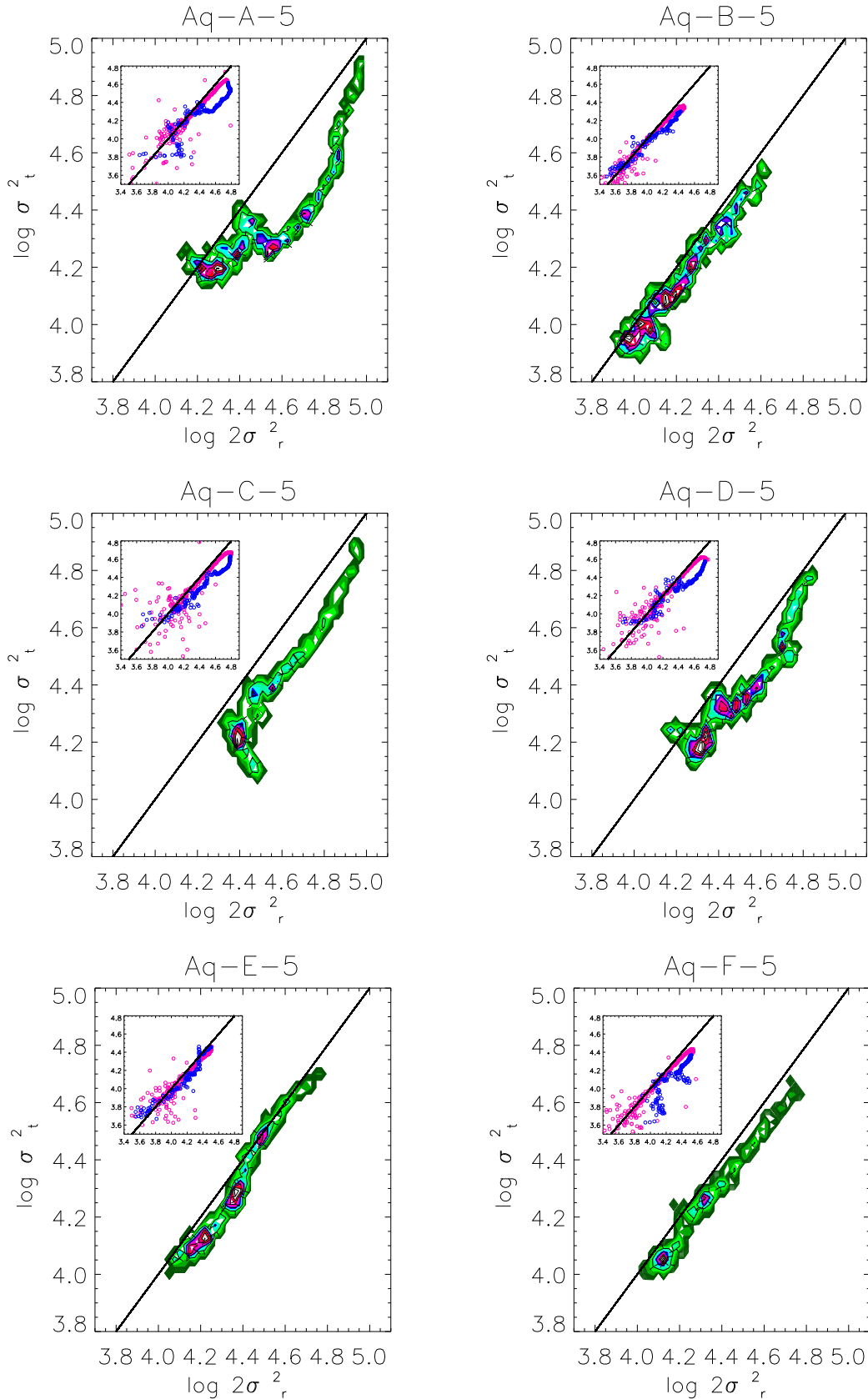


**Figure 4.** Tangential dispersion versus radial dispersion for the SPH haloes (velocities are in units of  $\text{km s}^{-1}$ ). The corresponding relations for the DM haloes of N08 are shown in magenta for  $2 h^{-1} \text{kpc} < r < r_{-2}$  and in blue for  $r_{-2} < r < r_{200}$  in the insets. The solid black line depicts equality. The SPH haloes show a monotonic relation with radius for both components with the higher dispersion values for smaller radius as shown in Fig. 2.



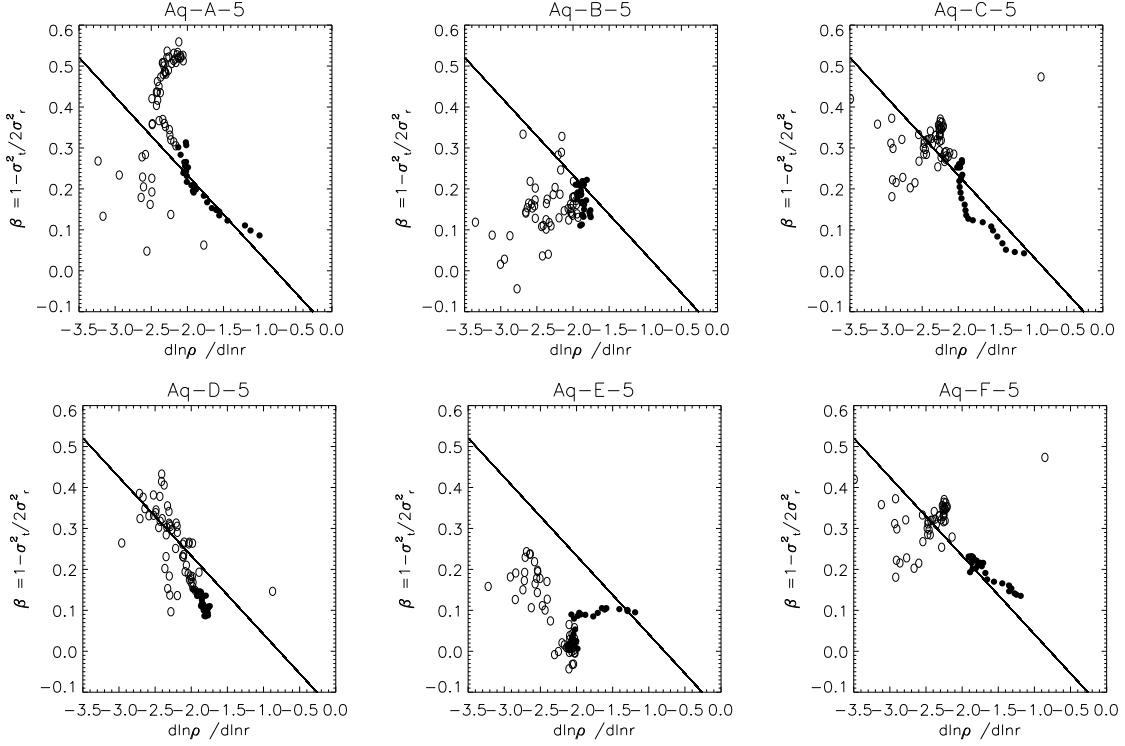


**Figure 5.** Velocity anisotropy  $\beta$  as a function of the local value  $\gamma$  of the logarithmic slope of the density profile in the SPH runs. Filled symbols correspond the radial range  $2 h^{-1} \text{kpc} < r < r_{-2}$  and open circles to the range  $r_{-2} < r < r_{200}$ . The Hansen & Moore (2006) relation is shown as a solid line.

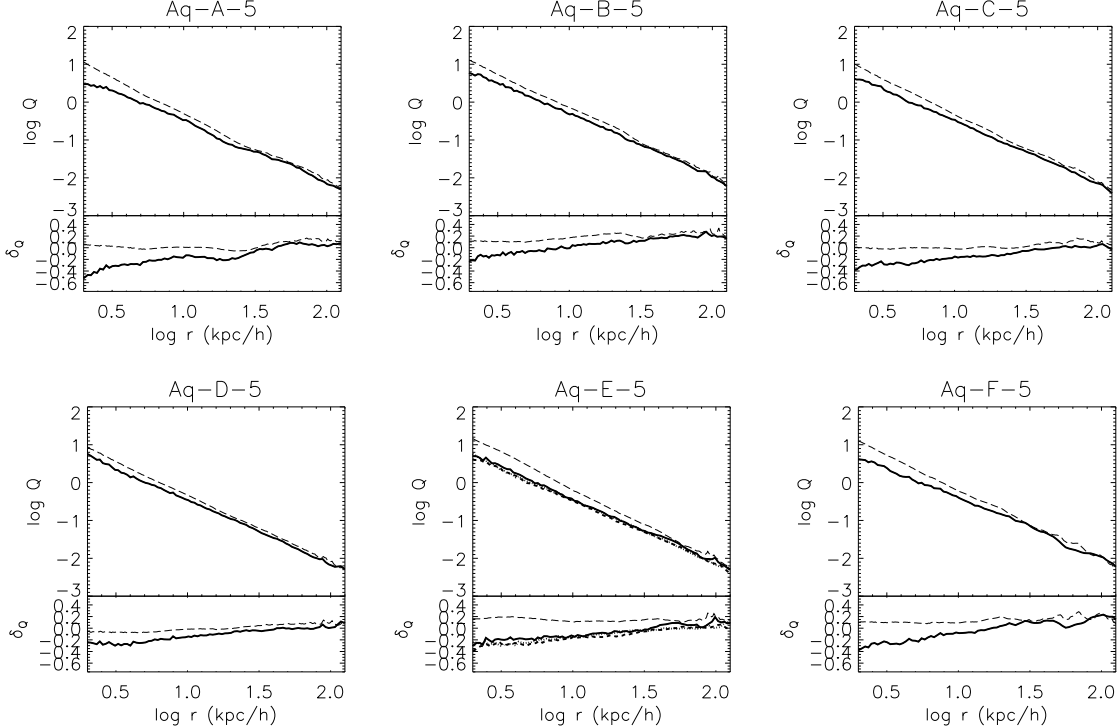


**Figure 6.** Pseudo-phase-space density profiles as a function of radius for haloes in the SPH (solid lines) and DM (dashed lines) runs ( $Q$  is in units of  $h^2 M_\odot \text{kpc}^{-3} (\text{km s}^{-1})^{-3}$ ). Residuals of the two relations from the power-law relation predicted in Bertschinger's (1985) similarity solution are shown in the narrow lower panels of each plot. We include the lower resolution versions of Aq-E: Aq-E-6 (short dashed lines) and Aq-E-7 (dotted lines).

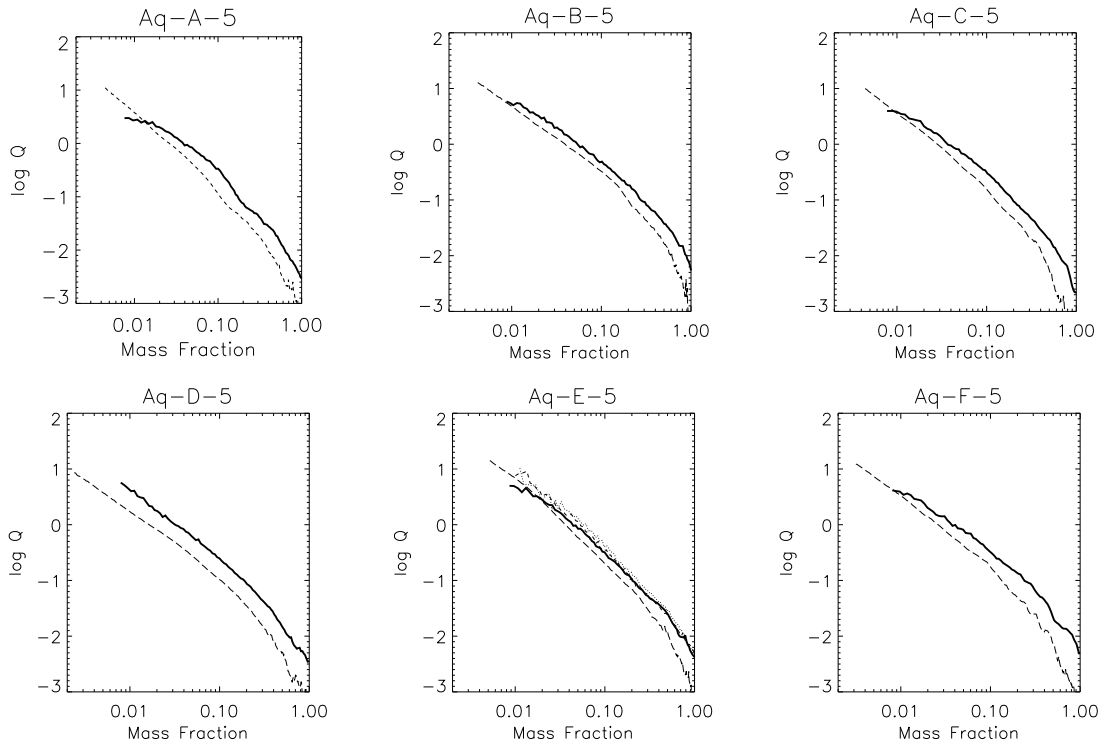


**Figure 7.** Pseudo-phase-space density profiles as a function of enclosed dark matter mass fraction for haloes in the SPH (solid lines) and DM (dashed lines) runs ( $Q$  is in units of  $h^2 M_\odot \text{kpc}^{-3} (\text{km s}^{-1})^{-3}$ ). The profiles are shown over the same radial range already shown in Fig. 6. We include the lower resolution versions of Aq-E: Aq-E-6 (short dashed lines) and Aq-E-7 (dotted lines).

## 6 SHAPES

Haloes formed by hierarchical clustering of dark matter in CDM scenarios are typically triaxial (e.g. Barnes & Efstathiou 1987; Frenk et al 1988; Jing & Suto 2002) with the inner regions being approximately prolate (e.g. Hayashi et al. 2007). However, when baryons condense to make galaxies in these inner regions they become rounder and approximately oblate (Dubinski 1994; Tissera & Domínguez-Tenreiro 1998; Kazantzidis et al. 2004). This latter result seems in better agreement with a variety of observational shape estimates for galaxy haloes (e.g., Sackett & Sparke 1990; Kuijken & Tremaine 1994; Koopmans et al. 1998; Helmi 2004; Weijmans et al. 2008). We measure the shapes of our SPH and DM haloes following the Dubinski & Carlberg (1991) method, based on the eigenvalues of the moment of inertia tensor,  $I$ . For each bin of  $N$  particles we computed ellipsoidal radii

$$r = [x^2 + \frac{y^2}{(b/a)^2} + \frac{z^2}{(c/a)^2}]^{1/2} \quad (1)$$

The semi-axes of the triaxial ellipsoids ( $a > b > c$ ) are calculated iteratively as

$$\frac{b}{a} = \left(\frac{I_{22}}{I_{11}}\right)^{1/2}, \frac{c}{a} = \left(\frac{I_{33}}{I_{11}}\right)^{1/2} \quad (2)$$

where  $I_{11} > I_{22} > I_{33}$  are the eigenvalues of the tensor of inertia ( $I_{jk} = \sum_i x_i^j x_i^k / r_i^2$ ). In order to determine  $a$ ,  $b$  and  $c$ , an iterative cycle is set up, starting with  $b/a = c/a = 1$ .

In Fig. 8 we show the axis ratios and the triaxiality parameter  $T$  defined as  $T = (a^2 - b^2)/(a^2 - c^2)$  as a function

of radius. Purely prolate objects have  $T = 1$ , while purely oblate ones have  $T = 0$ . In agreement with previous work, we find a general trend for the SPH runs to be more oblate than their DM counterparts. Although in all haloes both axis ratios increase at most radii, each halo shows its particularities. The largest change in shape occurs in Aq-C-5 which becomes oblate with  $T < 0.4$  over the whole analysed range. The smallest change in shape is found in Aq-F-5 which only weakly modifies its overall prolate shape, although the axis ratios do increase noticeably. The only galaxy without any disc component at all inhabits this halo. Halo Aq-E-5 shows a strong dependence of  $T$  on radius in the DM run, varying from  $T \approx 0.6$  to  $T \approx 0.1$ . This behaviour is preserved when baryons are included although the axis ratios do increase slightly. Interestingly, the galaxy in this halo is the only one with a strongly rotating bulge. Initially triaxial shapes become much more nearly oblate in the baryon dominated regions for Aq-A-5, Aq-B-5 and Aq-D-5. These haloes have galaxies with extended, diffuse surviving discs. For halo Aq-E we have included the analysis of the shapes for the two lower resolution versions in Fig. 8. In agreement with the other parameters, the shapes tend to converge as numerical resolution increases. As expected, the dark matter halo in the lowest resolution version, Aq-E-7, has the noisiest shape.

## 7 CIRCULAR VELOCITY AND THE ADIABATIC CONTRACTION MODELS

The adiabatic contraction (AC) hypothesis has been used extensively to model the effects that baryon condensation

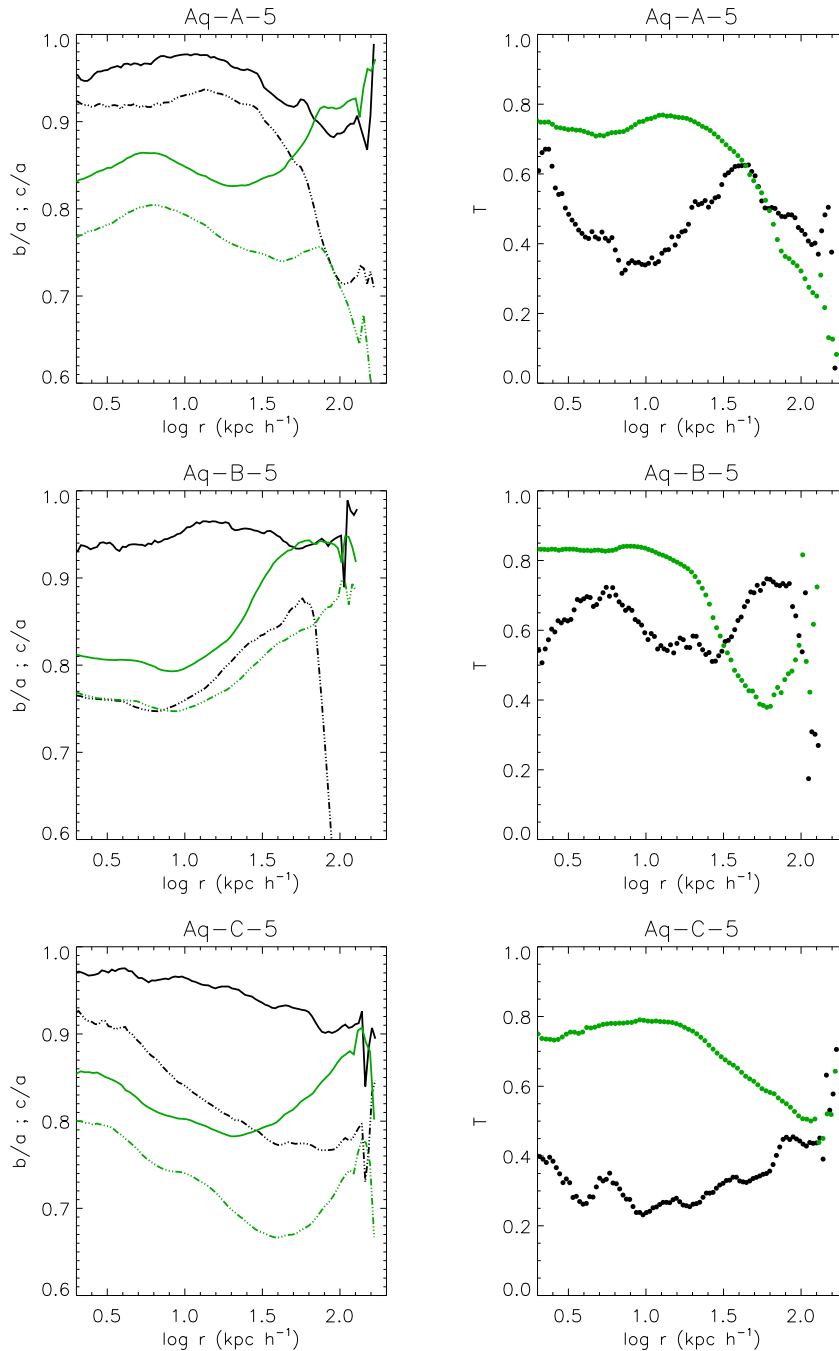


**Figure 8.** Axis ratios  $b/a$  (solid lines) and  $c/a$  (dotted-dashed lines) for haloes in our SPH (black) and DM (green) runs. In the right panels, the triaxiality parameter  $T$  is also shown;  $T = 0$  for oblate systems while  $T = 1$  for prolate ones. We include the lower resolution versions of Aq-E: Aq-E-6 (blue) and Aq-E-7 (red).

produces on dark matter haloes. As discussed in the Introduction, there is now a consensus that the simplest implementation of this hypothesis overestimates the dark matter concentration in the central region and makes it very difficult to reconcile observations with CDM models. This discrepancy may well reflect issues other than dark matter compression by baryonic gravity, but adopting an inappropriate AC hypothesis can certainly exacerbate the problem. In this section, we will apply the standard model of B86, the

modified algorithm of G04 and the statistical motivated relation of A09, comparing their predictions to our simulated dark matter circular velocity profiles.

The differences between these various recipes can be seen in Fig. 9. These plots show the directly measured dark matter circular velocities ( $V_c = [GM_{dm}(r)/r]^{1/2}$  where  $M_{dm}(r)$  is the dark matter mass enclosed within  $r$ ) in our SPH (red lines) and DM (black lines) simulations and compares them to the curves predicted by modifying the result

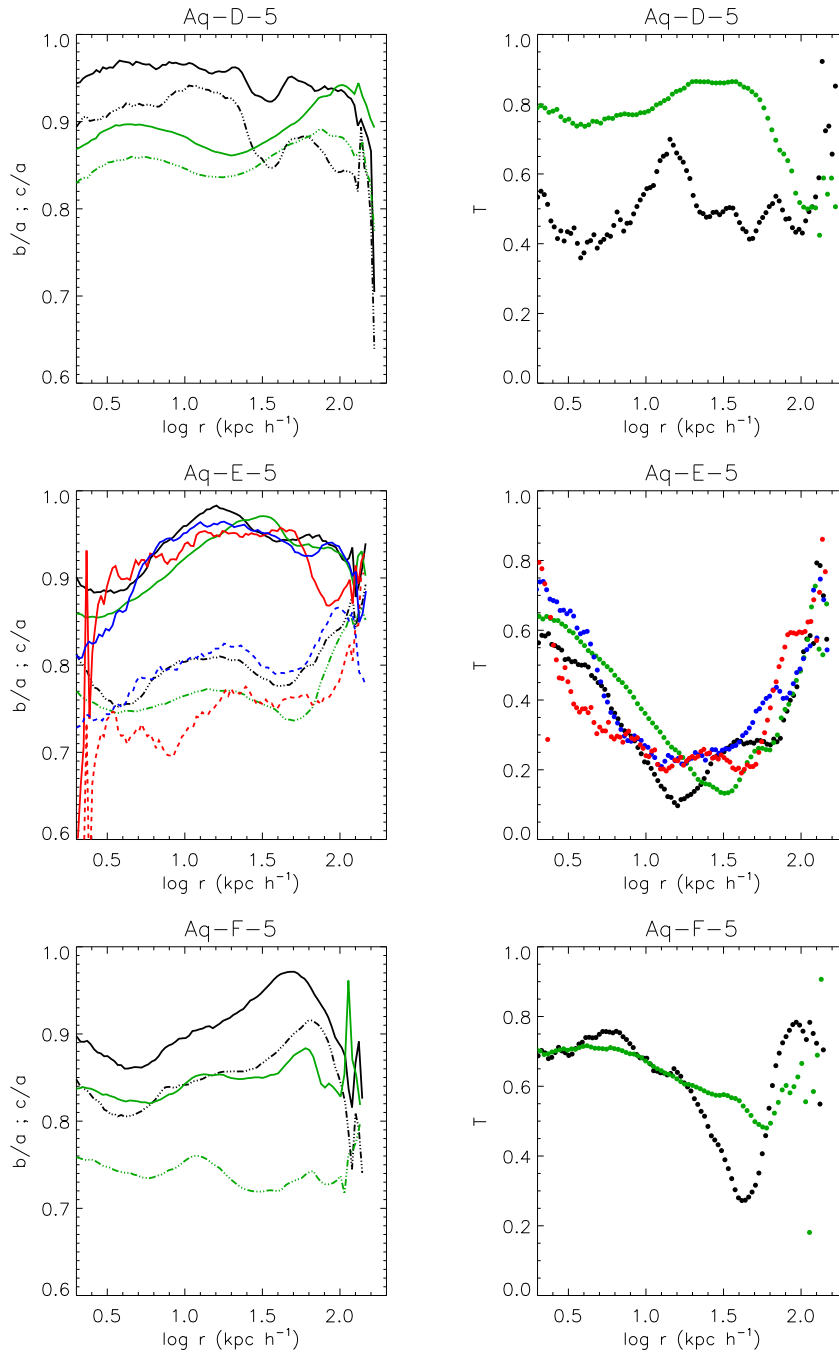
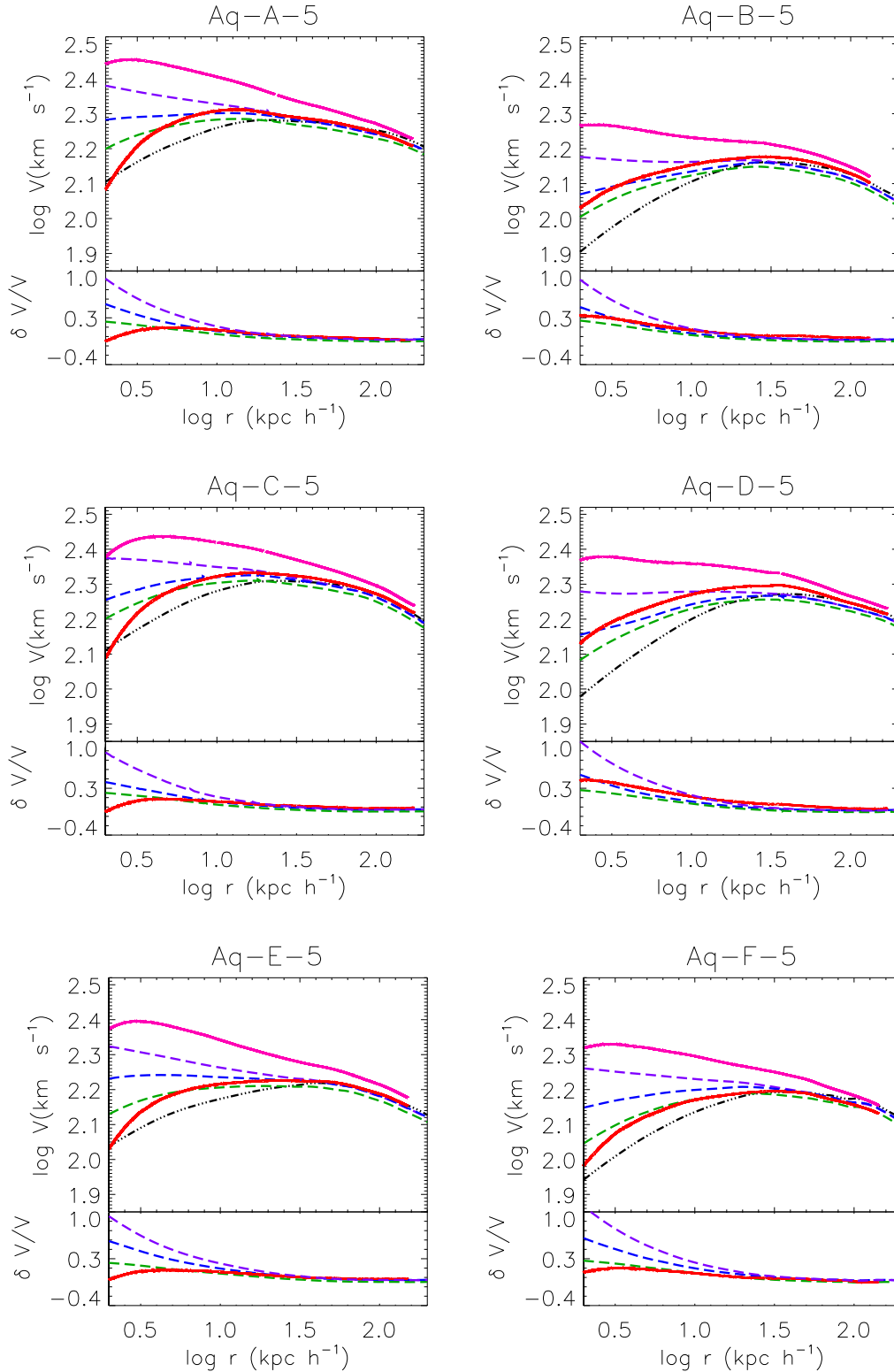


Figure 8 – continued

for the DM run according to each of the three recipes, assuming the baryon distribution found in the SPH run. The DM profiles have been reduced by 8% to account for the global baryonic fraction of 0.16 adopted in the SPH simulations. In the narrow panels at the bottom of each plot we show the residuals from the pure DM result for each of the models (the three dashed curves) and for the dark matter distribution actually found in the SPH simulation (the solid red curve). As expected, the AC model of B86 overpredicts the amount of dark matter in the central regions by up to 50% or so. The G04 and A09 models provide a better representation with A09 being closer to the “true” result in most cases. However, for two haloes (Aq-B-5 and Aq-D-5), the

A09 model underestimates the dark matter mass by several tens of percent at some radii. This is expected, since the Abadi et al (2009) prescription is based on a large sample of dark matter haloes, and for individual haloes one can expect overestimates and underestimates in roughly equal numbers, just as we find. Note that for Aq-B-5 and Aq-D-5 the G04 prescription actually gives the best description at all but the smallest radii.

In general terms, the dark matter mass in the innermost regions is usually overpredicted and, more importantly, the shape of the circular velocity is often poorly matched by all of these models. At least in three of our haloes (Aq-A-5, Aq-C-5 and Aq-E-5), the velocity curves rise in the



**Figure 9.** Dark halo circular velocity curves predicted by applying the AC models of Blumenthal et al. (1986, violet dashed lines), Gnedin et al. (2004; blue dashed lines) and Abadi et al. (2009, green dashed lines) to the circular velocity curves of our DM simulations assuming the central baryon distribution found in our SPH simulations. We also show the directly measured circular velocity curves in the SPH (red solid lines) and DM (black dotted-dashed lines) simulations. Thus if the AC models worked perfectly their curves would match the red solid lines. In the lower panels we show residuals of the three model predictions from the original DM curves, and compare them with the residuals for the actual curves in the SPH simulations. For this comparison, the curves for the AC models and DM simulations have been scaled down by 8% to account for the baryon fraction in the SPH simulations. We also show circular velocity curves for the total mass (DM + baryons) in the SPH runs (magenta lines).

central region more gently than predicted by the models (in agreement with Fig.1).

## 8 CONCLUSIONS

We have analysed the dark matter distributions in six galaxy-sized haloes belonging to the Aquarius Project, comparing results from the original dark matter only simulations to those from re-simulations including baryonic processes (S09). In agreement with previous work, we find that dark matter haloes become more concentrated when baryons condense at their centres, but that the characteristics of the contraction do not correlate in a simple way with the total amount of baryons. Our main contribution here is to analyse similar mass haloes with a variety of formation histories using high resolution simulations with and without baryons. Our results show that the response of haloes to the presence of baryons is sensitive to the details of halo assembly. This set of six galaxy-sized haloes provides the opportunity to study which properties can be considered common to such haloes and which depend significantly on their particular formation history.

Our findings can be summarized as follows:

- In the regions dominated by baryons, haloes become significantly more concentrated than their dark matter only counterparts. The level of concentration varies significantly from object to object, however, it is not simply related to the total baryonic mass accumulated in the central galaxy. For  $r < r_{-2}$ , the dark matter density profiles of many of our simulations are nearly isothermal except, possibly, very close to the centre.

- The velocity dispersion structure is modified in all haloes, with velocity dispersion increasing monotonically to small radii in all cases. The temperature inversion of NFW profiles is no longer present once the galaxy has formed. In some systems, the tangential dispersion increases more than the radial dispersion (but not all), causing them to become more nearly isotropic.

- The  $\beta$ - $\gamma$  relation proposed by Hansen & Moore (2006) is obeyed at most over a restricted radial range for some of our haloes. It works best in the central region of those systems where the isothermal behaviour extends over a relatively small range. The departures from their predictions become large when the profile is isothermal or has constant anisotropy over an extended radial range.

- Pseudo-phase-space density no longer follows the same power law in radius as in Bertschinger's (1985) similarity solution once galaxy formation is included. The profile differs from one halo to the next and in no halo is it consistent with the purely adiabatic contraction of the dark matter only case.

- As in previous work, the condensation of baryons makes the central regions of all our haloes less aspherical and more nearly oblate, although in two cases the changes are small. One of these has no significant disk component and the other has a bulge with substantial net rotation.

- None of the simple adiabatic contraction models proposed in earlier work is able to describe how the radial density profiles of our haloes are modified by baryon condensation. The scheme suggested by Abadi et al (2009; see also Pedrosa et al. (2010)) is the most successful of those

we consider, although it can significantly over- or underestimate the effects in individual cases. For the same haloes, the central mass is overestimated by more than 50%. The circular velocity curves of our galaxy formation simulations are not as centrally peaked as predicted by such adiabatic contraction models, but are still more rapidly rising than in many observed spirals. Since none of our simulated galaxies is disk-dominated it is unclear whether this is a problem.

Our analysis show that haloes of similar virial mass respond in different ways to baryon condensation depending on the details of their assembly history. Consequently, a much more detailed understanding of galaxy formation is needed before we can make reliable predictions for the detailed structure of the dark matter haloes surrounding galaxies.

## ACKNOWLEDGEMENTS

We thank the referee of this paper for her/his useful comments that helped to improved this paper. The simulations were carried out at the Computing Centre of the Max-Planck-Society in Garching. This research was supported by the DFG cluster of excellence 'Origin and Structure of the Universe'. PBT thanks the Max Planck Institute for Astrophysics (Garching, Germany) for its hospitality during her visits. This work was partially funded by PROALAR 07 (DAAD-Secyt collaboration), PICT 32343 (2005) and PICT Max Planck 245 (2006) of the Ministry of Science and Technology (Argentina).

## REFERENCES

- Abadi et al. 2009, *MNRAS*, submitted (A09)  
 Ascasibar, Y., Yepes, G., Gottlober, S., Muller, V. 2004, *MNRAS*, 352, 1109  
 Banes, J. & Efstathiou, G. 1987, *ApJ*, 319, 575  
 Bertschinger, E. 1985, *ApJS*, 58, 39  
 Blumenthal, G.R., Faber, S.M., Flores, R. & Primack, J.R. 1986, *ApJ*, 301, 27 (B86)  
 Boylan-Kolchin, M., Springel, V., White, S. D. M., Jenkins, A. & Lemson, G. 2009, *MNRAS*, 398, 1150  
 Debattista, V. P., Moore, B., Quinn, T., et al. 2008, *ApJ*, 681, 1076  
 Diemand J., Zemp, M., Moore B., Stadel, J., & Carollo, C., M. 2005, *MNRAS*, 364, 665  
 Dubinski, J., & Carlberg, R. G. 2008, *ApJ*, 378, 496  
 Dubinski, J. 1994, *ApJ*, 431, 617  
 Dutton, A.A., van den Bosch, F.C. & Courteau, S. 2008, *arXiv0801.1505*  
 Eggen, O.J., Lynden-Bell, D., & Sandage, A. R. 1962 *ApJ*, 136, 748  
 Einasto J. 1965, *Trudy Inst. Astrofiz. Alma-Ata*, 51, 87  
 Evrard, A. E., Summers, J. & Davis, M. 1994, *ApJ*, 422, 11  
 Flores, R. A. & Primack, J. R. 1994, *ApJ*, 427, L1  
 Frenk, C., S., White, S.D. M., Davis, M., & Efstathiou, G. 1998, *ApJ*, 227, 507  
 Gao, L., Navarro, J.F., Cole, S., Frenk, C., White, S.M.D., Springel, V., Jenkins, A., Neto, A.F. 2008, *MNRAS*, 387, 536  
 Gnedin, O.Y. Kravtsov, A., Klypin, A. & Daisuke, N. 2004, *ApJ*, 616, 16 (G04)  
 Hansen, S.H. & Moore, B. 2006, *NewA*, 11, 333  
 Hayashi, E., Navarro, J. F. & Springel, V. 2007, *MNRAS*, 388, 2

- Helmi, A. 2004, *MNRAS*, 351, 643
- Jing, Y. P. & Suto, Y. 2002, *ApJ*, 574, 538
- Katz, N. & Gunn, J. E. 1991, *ApJ*, 377, 365
- Kazantzidis, S., Mayer, L., Mastropietro, C., Diemand, J., Stadel, J., & Moore, B. 2004, *ApJ*, 608, 663
- Koopmans, L. V. E., de Bruyn, A. G. & Jackson, N. 1998, *MNRAS*, 295, 534
- Kuijken, K. & Tremaine, S. 1994, *ApJ*, 421, 178
- McGaugh, S. S. & de Blok, W. S. G. 1998, *ApJ*, 499, 41
- Mo, H. J. Mao, S. & White, S. D. M. 2001, *MNRAS*, 295, 319
- Moore, B., Ghigna, S., Governato, F., Lake, G., Quinn, T., Stadel, J. & Tozzi, R. 1999, *AJ*, 524, L19
- Mosconi, M., Tissera, P. B., Lambas, D. G. & Cora, S. A. 2001, *MNRAS*, 325, 34
- Navarro J. F., Frenk C. S. & White S. D. M. 1996, *ApJ*, 462, 563
- Navarro J. F., Frenk C. S. & White S. D. M. 1997, *ApJ*, 490, 493
- Navarro J. F., Ludlow, A., Springel, V., Wang, J., Vogelsberger, White S. D. M., Jenkins, A., Frenk C. S., Helmi, A. 2008, *MNRAS*, submitted (N08)
- Oñorbe, J., Domínguez-Tenreiro, R., Sáiz, A. & Serna, A. 2007, *MNRAS*, 376, 390
- Pedrosa, S., Tissera, P.B. & Scannapieco, C. 2009, *MNRAS*, 395, L57
- Pedrosa, S., Tissera, P.B. & Scannapieco, C. 2010, *MNRAS*, accepted
- Power, C. et al. 2003, *MNRAS*, 338, 14
- Rasia, E., Tormen, G. & Moscardini, L. 2004, *MNRAS*, 351, 237
- Romano-Díaz, E., Shlosman, I., Heller, C. & Hoffman, Y. 2008, *ApJ*, submitted
- Sackett, P. D. & Sparke, L. S. 1990, *ApJ*, 361, 408
- Salucci, P., Yegorova, I. A., Drory, N. 2008, *MNRAS*, 388, 159
- Scannapieco C., Tissera P.B., White S.D.M. & Springel V. 2005, *MNRAS*, 364, 552
- Scannapieco, C., Tissera P.B., White S.D.M. & Springel V. 2006, *MNRAS*, 371, 1125
- Scannapieco, C. Tissera, P.B., White S.D.M. & Springel V. 2008, *MNRAS*, 389, 1137
- Scannapieco, C., White S.D.M., Springel V. & Tissera, P.B. 2009, *MNRAS*, 396, 696 (S09)
- Sellwood, J. A. & MacGaugh, S. S. 2005, *ApJ*, 634, 70
- Springel V. et al. 2008, *MNRAS*, 391, 1685
- Taylor, J. E. & Navarro, J.F. 2001, *ApJ*, 563, 483
- Tissera, P. B. & Domínguez-Tenreiro, R. 1998, *MNRAS*, 297, 177
- Vass, I. M., Valluri, M., Kravtsov, A. V. & Kazantzidis, S. 2008, *MNRAS*, astro-ph. 0810.0277
- Vogelsberger, M., Helmi, A., Springel, V., White, S. D. M., Wang, J., Frenk, C. S., Jenkins, A. et al. 2008, *MNRAS*, 395, 797
- Weijmans, A. M., Krajnovic, D., van de Ven, G., Oosterloo, T. A., Morganti, R. & de Zeeuw, P. T. 2008, *MNRAS*, 383, 1343
- Zeldovich, Y. b., Klypin, A.A., Khlopov, M. Y., & Checherkin, V. M. 1980, *Soviet J. Nucl. Phys*, 31, 664